THE JOURNAL OF PHYSICAL CHEMISTRY C
A JOURNAL OF THE AMERICAN CHEMICAL SOCIETY

pubs.acs.org/JPCC

Article

Machine Learning Analysis of Reaction Parameters in UV-Mediated Synthesis of Gold Nanoparticles

Alexander A. Guda,* Mikhail V. Kirichkov, Viktor V. Shapovalov, Alexey I. Muravlev, Danil M. Pashkov, Sergey A. Guda, Anton P. Bagliy, Sergey A. Soldatov, Sergey V. Chapek, and Alexander V. Soldatov

Cite This: https://doi.org/10.1021/acs.jpcc.2c06625

Read Online

ACCESS | Metrics & More | Article Recommendations | Supporting Information

ABSTRACT: Gold nanoparticles represent an important class of functional nanomaterials for optoelectronics, biomedical applications, and catalysis. Therefore, controllable synthesis of nanoparticles with specified size and shape is important. Though reduction of gold ions is quite a simple process and may be performed with many different protocols, the reproducibility of the results and transfer of protocols between independent research groups remains a challenging task. Machine learning analysis based on statistical approaches is hardly applicable to the published data, since most of the researchers report only successful syntheses. In this work, we apply uniform sampling of the reaction parameter space. The concentrations of gold precursor, reducing agent, and surfactant were varied via an improved Latin hypercube sampling, and each run was performed under in situ UV−vis control. Based on the resulting set of optical spectra, we address the relevant chemical questions about nanoparticle formation, their shape, and period of growth. Our work demonstrates a data driven approach applied to the space of reaction parameters in a limited available set of experiments.

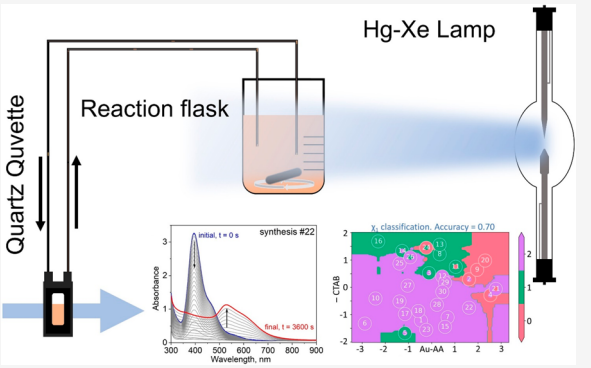

1. INTRODUCTION

Metal nanoparticles (NP) find their numerous applications in different fields of fundamental research,[1] industry,[2] and medicine[3,4] due to their unique optical properties,[5] electronic structure, tunable surface sites for catalytical reactions,[6−8] and antibacterial and anticancer effects.[9,10] The gold nanoparticles represent a unique case that combines all these properties. They can be synthesized in different sizes and shapes[11−14] that are appropriate, e.g., for the task of dye photodegradation,[15] local electromagnetic field generation,[16] and molecular sensors.[17]

The most common method for synthesis reported in the literature is the preparation of spherical nanoparticles with the Turkevich protocol[18−20] where sodium citrate reduces Au^{3+} ions from the $HAuCl_4$ precursor and stabilizes nanoparticles in aqueous medium. The wide range of sizes and shapes of colloidal gold nanoparticles are produced by combining different gold salt precursors, surfactants reducing agents,[21−26] use of seeds[27] and external stimuli.[28] Photochemical synthesis under ultraviolet irradiation produces reductive species with spatiotemporal control and helps to avoid toxic reagents. Ohara et al.[29] demonstrated seed-mediated Au nanoparticles synthesis via the hydroquinone/benzoquinone photochemical redox system. The diameter of the formed AuNPs depended on the concentration of seed particles, with a higher seed particle concentration yielding smaller nanoparticles. Chloroauric concentration and pH make a great influence on the geometry of the nanoparticles as demonstrated by Rodríguez et al.,[30] in photochemical synthesis. Gold nanorods are often synthesized in a presence of CTAB, Ag ions and seeds.[31] Song et al. synthesized gold nanorods with controlled aspect ratios through a simple photochemical process using silver nitrate.[32] The amount of silver ions added to the system dictates the aspect ratio of the final rods. However the presence of silver ions in the reaction mixture may lead to the bimetallic nanoparticles. Sortino et al.[33] report on a effective preparation of Ag, Au, and Au@Ag core−shell nanoparticles based on the light irradiation of a biocompatible, water-soluble dextran functionalized with benzophenone in the presence of $AgNO_3$, $HAuCl_4$, or both.

The complex interplay between nucleation and growth of existing seeds in the solution makes colloidal synthesis difficult to tune. The reagent concentrations, their order, and temperature influence the resulting size and shape distribution.[34−36] Minor changes in the protocol may affect the

Received: September 16, 2022
Revised: December 18, 2022

Table 1. List of 30 Points Generated According to the IHS Scheme for Three Reaction Parameters[a]

synthesis #	Au, mol	ascorbic acid, mol	CTAB, mol	Au, normalized	ascorbic acid, normalized	CTAB, normalized
1	0.079	0.065	0.0077	−0.404	0.058	1.218
2	0.133	0.045	0.0039	1.098	−0.519	−0.290
3	0.116	0.089	0.0033	0.635	0.750	−0.520
4	0.124	0.005	0.0054	0.866	−1.675	0.289
5	0.104	0.112	0.0089	0.289	1.444	1.676
6	0.050	0.120	0.0080	−1.213	1.675	1.327
7	0.095	0.041	0.0074	0.057	−0.635	1.097
8	0.070	0.029	0.0016	−0.635	−0.983	−1.208
9	0.112	0.013	0.0030	0.520	−1.444	−0.640
10	0.046	0.101	0.0057	−1.328	1.098	0.409
11	0.145	0.077	0.0028	1.444	0.404	−0.749
12	0.054	0.009	0.0036	−1.098	−1.560	−0.400
13	0.099	0.057	0.0007	0.173	−0.173	−1.558
14	0.033	0.049	0.0013	−1.675	−0.404	−1.328
15	0.137	0.085	0.0083	1.213	0.635	1.447
16	0.041	0.093	0.0004	−1.444	0.866	−1.678
17	0.062	0.073	0.0071	−0.866	0.289	0.977
18	0.128	0.116	0.0068	0.982	1.560	0.868
19	0.091	0.109	0.0060	−0.057	1.329	0.518
20	0.149	0.037	0.0022	1.560	−0.750	−0.979
21	0.153	0.025	0.0048	1.675	−1.098	0.059
22	0.141	0.053	0.0065	1.328	−0.288	0.748
23	0.037	0.017	0.0086	−1.560	−1.329	1.556
24	0.120	0.097	0.0010	0.751	0.983	−1.448
25	0.087	0.105	0.0025	−0.173	1.214	−0.869
26	0.066	0.069	0.0019	−0.751	0.173	−1.099
27	0.075	0.081	0.0045	−0.520	0.519	−0.061
28	0.058	0.021	0.0063	−0.982	−1.213	0.638
29	0.083	0.033	0.0042	−0.289	−0.867	−0.170
30	0.108	0.061	0.0051	0.404	−0.058	0.169

[a]The following ranges were used: $HAuCl_4 \cdot 4H_2O$ [10−65 mg], L-ascorbic acid [0−25 mg], and CTAB [0−3.5 g]. Normalization was applied to each column and included subtraction of the mean across the column and division by the standard deviation of the mean.

resulting particle size distribution and increase the role of the human operator performing the reaction.[37] Machine learning (ML) methods address these challenges in a systematic statistical way.[38] ML combines exploration of the space of parameters to create the training set and estimates the quality of the approximation models via the cross-validation approach. Automated systems ensure stable and unbiased data collection and thus promote the ML-based approach.[39] The trained models after validation, can predict the result of the synthesis in terms of nanoparticle size, polydispersity, and aspect ratio.[40] Furthermore, they are implemented in the reverse engineering approach to predict the optimal synthesis parameters for the required product characteristic.[41]

The wide application of the ML models is hindered by the availability of synthesis databases. Most publications report only successful results while omitting the faults. Such an approach makes it difficult to apply ML methods to published works. Another issue concerns the complete description of the experimental protocol that may depend on the operator skills. Burrows et al.[37] applied composite fractional factorial analysis to the series of synthesis performed by different researchers in his group. The aim was to understand the of role of silver ions in the gold nanorods synthesis. The authors found that ascorbic acid influenced the intrinsic growth rates while silver nitrate and reaction temperature affected the length of the nanorods. They highlighted the importance of freshly prepared silver nitrate and ascorbic acid solutions to avoid photodegradation. Gherman et al. trained a neural network with three inputs ($HAuCl_4$:citrate ratio, light intensity, and light scanning velocity) to predict the spectral position of surface plasmon resonance (SPR) of gold nanoparticles in photochemical synthesis.[42] The radiation intensity was found to have the most important influence on the size distribution, followed by the scanning velocity and the citrate to gold(III) ratio. Li et al.[43] trained SNN (Siamese Neural Networks) stacked with the Graph Convolutional Neural Networks (GCNN) to perform a classification task for atomically precise Au nanoclusters. With the GCNN + SNN model, they were able to learn the relationship between reaction conditions, molecular properties, and the final monodispersity in the product.

Synthesis validation relies upon accurate diagnostics. Optical absorption of colloidal gold is characterized by a pronounced peak of plasmon resonance with the shape and position well correlated with the size and shape of these nanoparticles.[44] The shape of the spectrum is sensitive to the intermediate stages of the nanoparticle formation and provides complementary information to DLS,[45] small-angle X-ray scattering[46] and X-ray absorption spectroscopy[47] for the in situ monitoring of the reaction. Quantitative analysis of plasmon resonance characteristics in optical spectra can be performed by ML analysis based on accurate theoretical training sets.[48] In this work, the space of parameters for the photoassisted synthesis of gold nanoparticles was sampled via improved Latin hypercube sampling. We have applied UV−vis spectroscopy

https://doi.org/10.1021/acs.jpcc.2c06625
J. Phys. Chem. C XXXX, XXX, XXX−XXX

as an in situ probe of the whole reaction cycle and addressed chemical questions via the machine learning approach. The goal was to extract relevant information by using a small data set that is insufficient to train complex models with data of high dimensionality. The use of the Extra Trees algorithm permitted using small training sets and avoided overfitting. The algorithm was trained to find relationships between the descriptors of the UV−vis spectra and descriptors of synthesis. Good quality was obtained for the classification tasks for favorable conditions for the formation of NPs, their shape, and reaction time. Dimensionality reduction improved the quality of prediction and helped to visualize ML results which are usually reported as a black box methodology.

2. METHODS

2.1. Synthesis and Diagnostics. Reagents $HAuCl_4{\cdot}4H_2O$ ($HAuCl_4$ in the text for simplicity) and CTAB (hexadecyltrimethylammonium bromide) were purchased from Alfa Aesar. Cyclohexane was purchased from Labsolute-Chemsolute. Ascorbic acid (AA) was purchased from Sigma-Aldrich. Ultrapure water (18 MΩ·cm) was produced by the SimplicityUV system (Millipore) from distilled water.

Gold nanoparticles of different shapes were synthesized according to the protocol described in ref 49. In a typical synthesis, 20 mL of an aqueous solution of the $HAuCl_4{\cdot}4H_2O$, 40 mL of an aqueous solution of the CTAB, 0.34 mL of an aqueous solution of the L-ascorbic acid, 4 mL of a 1.4 mM aqueous solution of the $AgNO_3$, 1.35 mL of acetone, and 0.9 mL of cyclohexane were mixed in a quartz vessel. Masses of gold precursor, CTAB, and ascorbic acid in the constant corresponding volumes of water were varied in each reaction according to the Table 1. Synthesis was carried out for 60 min under UV radiation using a Newport 66901 setup with an Oriel Instruments 66142 Mercury−xenon lamp with a power of 386 W without filters. A 100 mL quartz vessel was placed 25 cm apart from the lamp. The irradiation area was approximately 14 cm^2. A magnetic stirrer on the bottom of the reaction vessel ensured homogeneous mixing along the reaction.

During the synthesis, the small volume of the reaction mixture was instantaneously pumped through a flow cell with a 5 mm optical path in a two-beam spectrophotometer SHIMADZU UV-2600 to record optical absorption spectra in situ. Acquisition time for each spectrum was 102 s and 35 spectra were measured in total during the synthesis (Figure S2 in Supporting Information). A scheme of the experimental setup is shown in Figure 1. For transmission electron microscopy analysis (Figure S3 in Supporting Information), the solution was centrifuged 3 times at 14000 rpm for 15 min. The precipitate was then dissolved in water.

2.2. Machine Learning Methods. In the research, we work with a relatively small amount of experimental data. Therefore, for both regression and classification tasks, the Extra Trees method[50] was applied with the following parameters: n_estimators = 100, max_depth = unlimited, min_samples_leaf = 1, min_samples_split = 2, and bootstrap = False. It is an ensemble ML method that combines the predictions obtained from many decision trees. In the case of classification the prediction is made by majority voting and in the case of regression—by averaging. The Extra Trees machine learning algorithm uses the whole original sample instead of bootstrap replicas and randomly chooses the cut points to split the nodes upon tree construction. These approaches motivate the reduction of both bias and variance. Another advantage of this method is the low computational cost, which allows iteration over many combinations of the descriptors during the search for optimal ones for high prediction quality.

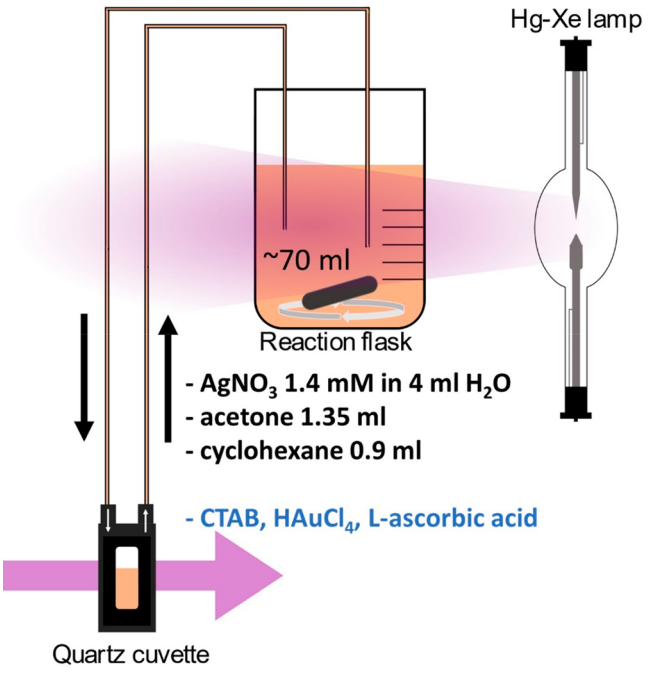

Figure 1. Scheme of the experimental setup. Amounts of $AgNO_3$, acetone, and cyclohexane precursors were fixed in all synthesis, while CTAB, $HAuCl_4 \times 4H_2O$ and L-ascorbic acid were varied according to Table 1.

To evaluate the quality of the predictions for classification the accuracy metrics was used in a Leave-One-Out cross-validation (LOOCV) procedure. Accuracy is determined as the ratio of correct predictions to the total number of objects in the data set. LOOCV is a reliable and unbiased estimate of model performance that is is optimal in the case of a small training data set. In the case of LOOCV, we sequentially exclude one object from the training sample for prediction and use the rest as a training sample. The learning task is to train the machine learning model that provides the highest LOOCV value:

$$\mathrm{LOOCV}(\mu, X^L) = \frac{1}{L}\sum_{i=1}^{L} \left\| \mu(X^L/x_i) - y_i \right\| \quad (1)$$

where μ is the machine learning algorithm, trained on the data set X^L consisting of features x_i and labels y_i. In our case, x_i are the descriptors of the synthesis and y_i are the descriptors of the spectra. On a small data set, the cross-validation quality depends on the initial random choice of the cut points in a tree; thus, for each target property y, we repeated the LOOCV five times and evaluated the average accuracy.

3. RESULTS AND DISCUSSION

3.1. Diversity of the Resulting Particles. The growth of gold nanoparticles depends on many parameters affecting reaction rates and preferable pathways. We have studied the dependence of the reaction on the three parameters: the amount of gold precursor, surfactant, and reducing agent. Experiments should properly sample the space of the parameters. When the sampling points in the space of

https://doi.org/10.1021/acs.jpcc.2c06625
J. Phys. Chem. C XXXX, XXX, XXX−XXX

parameters are generated by the researcher, it is important to make a highly representative data set and improve the generalizing ability of the machine learning model. Classical approaches to generation of the points distribution such as random and uniform meshing are not able to provide a homogeneity, especially in the case of a small data set. To solve this issue, we used the Improved Latin Hypercube Sampling method (IHS). IHS spreads out the points as evenly as possible with respect to their projections on each coordinate axis. The points generated by the IHS approach have smaller distances between the projections along each dimension compared with grid sampling. Table 1 shows amounts of three reagents in the synthesis generated according IHS sampling.

Figure 2 shows three representative series of UV−vis spectra measured during the syntheses #2, #22, and #25. The $HAuCl_4$ aqueous solution exhibits a UV−vis absorption peak at 313 nm due to metal-to-ligand charge transfer.[51] In the presence of CTAB, the four chloride ligands in $[AuCl_4]^-$ are replaced by bromide ions from the surfactant.[52,53] The resulting $[AuBr_4]$ complex has an absorption band at 400 nm obvious at the initial stage of the reaction (blue curve in Figure 2a). The further reaction pathway may be divided into two stages. The first stage is characterized by decoloration of the solution due to the reduction of Au^{III} to the Au^{I} complex.[53,54] The second stage is associated with the formation of the SPR peak of the metallic gold nanoparticles. In the synthesized particles, the spectrum may contain a single absorption maximum around 525 nm that is characteristic for the spherical particles (e.g., synthesis #25 in Figure 3) or several maxima beyond 525 nm characteristic for elongated particles (e.g., synthesis #3, #5, and #22 in Figure 3).[55]

The rate of the nanoparticle formation was also different across the series of reactions in Table 1. Figure 2c is an example of the slow synthesis when first stage of the decoloration was not completed during the observation period. A wide range of reagent concentrations and their independent variations in the series of synthesis generated several examples (synthesis #2, #9, #20, and #24) with such a behavior. On the contrary in Figure 2b, the first stage was so fast that it was not registered within the time resolution of the UV−vis measurements. Figure 2a is an intermediate case when durations of the both stages are comparable.

Figure 3a shows the resulting spectra in all syntheses measured after 1 h from the beginning. All spectra may be divided into three classes. The upper curves 2, 9, 20, and 24 contain negligible contribution from the Au SPR and are characterized by an intense maximum at 400 nm remaining from the Au^{III}−Br complex in the first stage of the reaction. TEM images for the reaction mixture #2 after 1 h from the start indicate branched nanowire network composed of nanoparticles and polymeric shell (Figure 4 in the main text and Figure S3 in Supporting Information). Such networks were previously observed in classical citrate-based synthesis[56] at the initial stage of the reaction. On the contrary, reaction mixture #20 with smaller amount of CTAB and ascorbic acid with respect to mixture #2 contained a sediment with larger particles up to 100 nm.

The bottom group of spectra (8, 11−14, 16, 17, 23, 25, 27, 28) is characterized by a single peak at 525 nm and thus can be described by a shape close to the spherical. TEM analysis of the mixtures with sharp spectral maximum confirms the quasi-spherical shape distribution for mixtures 11, 13, and 25 with

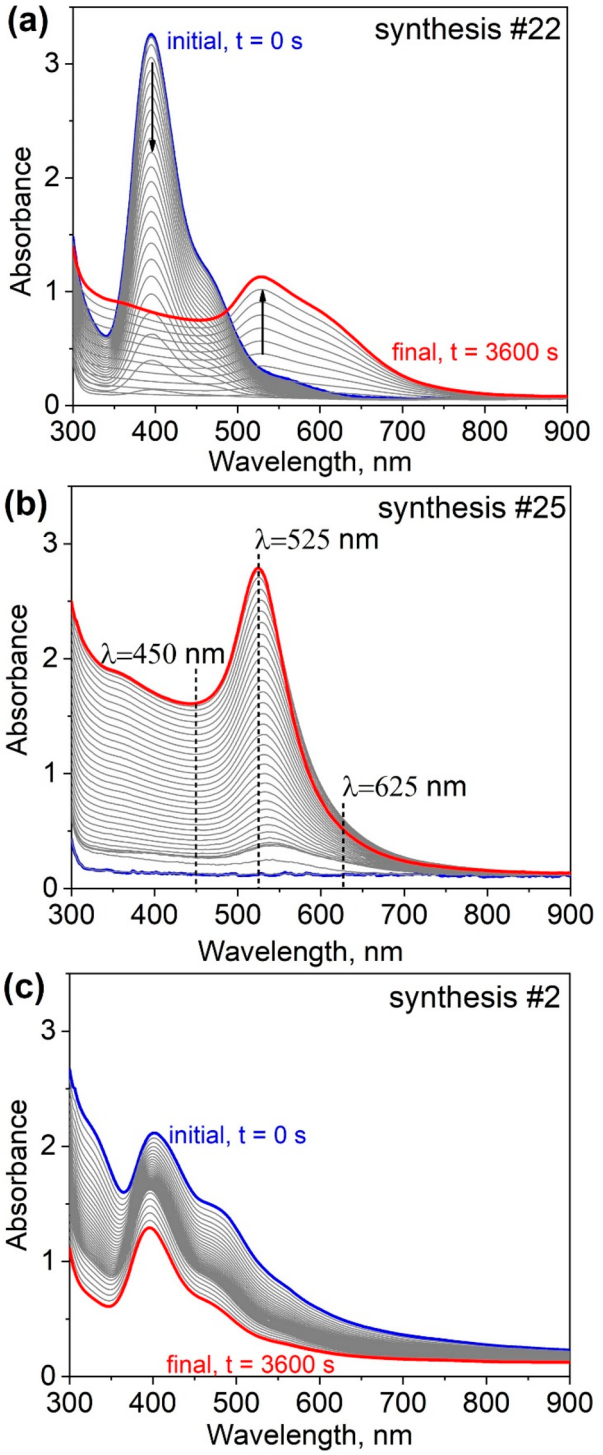

Figure 2. Representative series of UV−vis spectra measured in situ during three synthesis are reported in Table 1.

the average sizes 18, 15, and 10 nm correspondingly. The smallest dispersion of size distribution, 5 nm at FWHM, was observed for synthesis #11. In general, the presented distributions in Figure S3 are broad if compared to the carefully optimized synthesis condition, but such optimization was not the goal of the present study.

The rest of the UV−vis spectra in Figure 3a contain two maxima in the region of 500−700 nm. Figure 3b shows theoretical series of spectra for rod-shaped particles with

https://doi.org/10.1021/acs.jpcc.2c06625
J. Phys. Chem. C XXXX, XXX, XXX−XXX

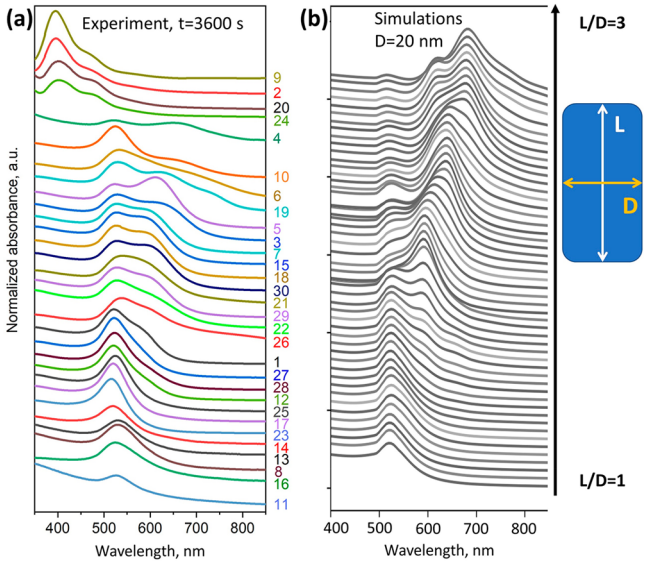

Figure 3. (a) Last experimental absorption spectra in in the series of in situ UV−vis measurements for each synthesis from Table 1. The spectra were normalized to their value at 450 nm and afterwards shifted vertically for clarity. (b) Theoretical calculations for the elongated nanoparticles with the aspect ratio L/D varied from 1 to 3.

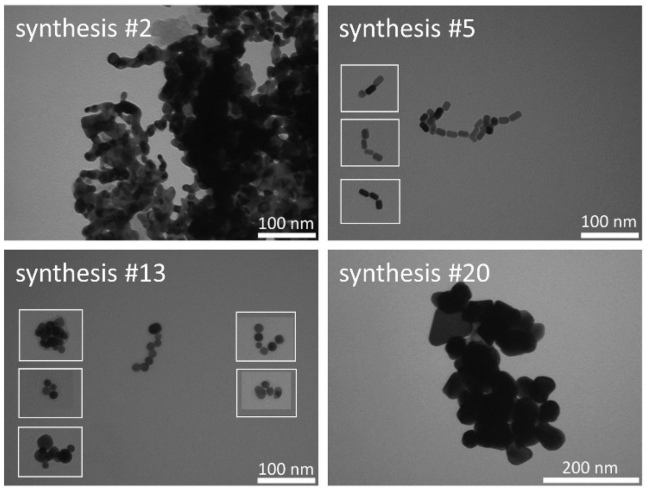

Figure 4. Representative TEM images for the particles synthesized with different concentration of reagents. Solutions #2 and #20 contain large signal from the unreacted Au^{III}−Br complex in UV−vis spectra, solution #13 has a single maximum at plasmon resonance frequency, solution #5 is characterized by an asymmetric plasmon band with two maxima. White rectangles mark compilations of frames from several TEM images of the same sample.

different aspect ratio according to the methodology in.[48] Simulations explain additional feature at ∼600 nm as elongated shape of gold nanoparticle with an aspect ratio $1 < L/D < 3$. TEM images of samples from syntheses #3, 5, 7, and 22 clearly indicate rod like shape of the resulting particles in agreement with the spectroscopic conclusions. In the next sections, we perform classification of the resulting spectra and find the relationship between spectral shape and parameters of the synthesis.

3.2. Descriptors of Spectra and Descriptors of Synthesis. The peculiarity of the complex reactions studied in the laboratory conditions is the limited amount of data for analysis compared to the synchrotron or X-ray free electron laser experiments. Therefore, the ML approximation model with low bias and variance should be constructed with preprocessed, but not raw data. Specific features of spectra which are the most sensitive to the studied properties are called descriptors. Few such descriptors efficiently reduce the dimensionality of the data,[57] make the prediction clear for interpretation, and useful for chemical insights. Figure 5 compares two approaches for training the algorithm. In this work, we will construct an approximation between descriptors of synthesis and descriptors of spectra.

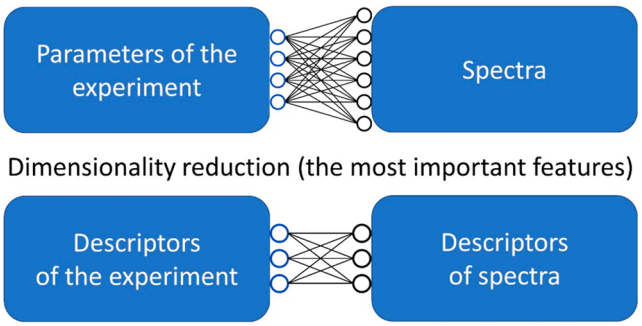

Figure 5. Comparison between two ML approximations based on raw data and the selected features (descriptors).

The intensity of the surface plasmon resonance (SPR) around 525 nm in the UV−vis absorption spectrum signalizes about the gold nanoparticles in the solution. Haiss et al.[44] introduced descriptor equal to the ratio of absorbances at SPR wavelength and 450 nm: $A(\mathrm{SPR})/A(450)$ that is linearly proportional to the logarithm of the NPs diameter. When the particles have rod-like shape they contain two maxima in the spectrum associated with the resonant absorption along dimension D and dimension L[58] as demonstrated in in Figure 3 (see also ref 48). To classify the series of experimental spectra in Figure 3, we selected two descriptors:

$$\chi_1 = A(525)/A(450) \tag{2a}$$

$$\chi_2 = A(625)/A(525) \tag{2b}$$

The χ_2 ratio measures the asymmetry of the SPR peak and within the observed range of nanoparticles signals about their nonspherical shape. Figure 6 shows scatter plots for the synthesis in the space of reaction parameters where color indicates the value of the spectra descriptors. The colors in panel a refer to the normalized intensity of the SPR maximum in the spectrum. The bottom right corner of the scatter plot contains points with low values of χ_1. These points are characterized by a larger amount of gold precursor and a smaller amount of reducing agent. The excessive amount of CTAB surfactant (compare points 21 vs 20, 4 vs 9, or 22 vs 2) favors the formation of nanoparticles even in the lack of ascorbic acid. The largest values for χ_1 are observed for points lying on the diagonal with equal molar amounts of gold precursor, ascorbic acid and sufficient amount of CTAB.

Descriptor χ_2 is visualized in Figure 6b. Lower values of χ_2 correspond to the spherical nanoparticles, while larger ones correspond to the rod-like geometry. The crossed-out points indicate the synthesis with no particles formed (black points in Figure 6a). In general, larger deviations from the spherical shape are observed for larger concentrations of the gold precursor or a greater contribution of ascorbic acid + CTAB in

https://doi.org/10.1021/acs.jpcc.2c06625
J. Phys. Chem. C XXXX, XXX, XXX−XXX

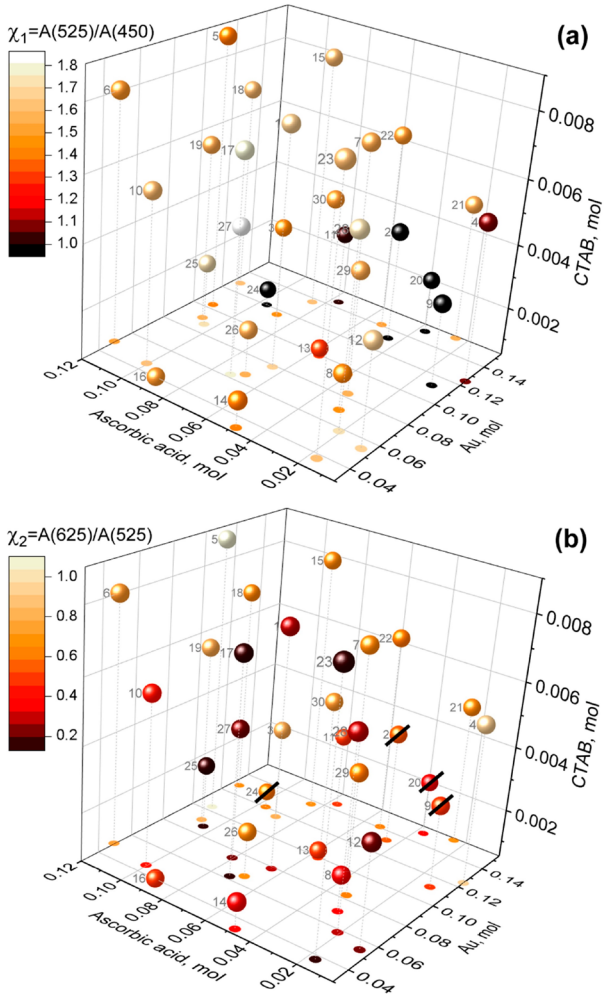

Figure 6. Scatter plots for the descriptors of spectra in the space of variable amounts of gold precursor $HAuCl_4 \cdot 4H_2O$, reducing agent ascorbic acid and surfactant CTAB. The color indicates the value of the corresponding descriptors χ_1 (panel a) and χ_2 (panel b).

the reaction mixture. In the following sections, we apply machine learning analysis to the observed quantities. The UV−vis spectrum of gold nanoparticles may have a nonlinear dependence on the synthesis parameters. Since our training sample is small, we construct different descriptors of synthesis and test their quality in the cross-validation procedure. Design of new descriptors is motivated by the search for the most informative ones for the ML method and those that improve performance of trained model. The list of descriptors is described in Table 2.

By training the ML model, we address the following questions related to the nanoparticle synthesis: if the nanoparticles were formed during the synthesis, what was the shape of the nanoparticles and the time of their formation. Table 3 combines the raised questions with the spectroscopic features.

Question 3 addresses the induction period of nanoparticle formation. We can follow size of gold NPs using the evolution of descriptor χ_1 as shown in Figure 7. Three colored spectra indicate different types of the reaction. The red one (representative synthesis #10) is characterized by fast decoloration and subsequent high rate of the SPR formation. The blue one (representative synthesis #22) is an example of

Table 2. Descriptors of spectra and descriptors of synthesis applied for training the Extra Trees Model

descriptor	comment
spectra	
$\chi_1 = A(525)/A(450)$	normalized height of the SPR maximum
$\chi_2 = A(625)/A(525)$	asymmetry of the SPR maximum
Synthesis	
Au, AA, CTAB	variable components in the synthesis
$c_1 \cdot$Au + $c_2 \cdot$AA + $c_3 \cdot$CTAB; $c_i = \pm 1$	linear combinations of initial parameters
Au·AA, Au·CTAB, AA·CTAB	products of the initial parameters

Table 3. Translating the Chemical Questions about the Synthesis into Classification Problems for the Descriptors of Spectra

question	descriptor of spectrum	classification
1. if the nanoparticles were formed during the synthesis	$\chi_1 = A(525)/A(450)$	class 0: $\chi_1 < 1$
		class 1: $1 < \chi_1 < 1.5$
		class 2: $\chi_1 > 1.5$
2. spherical or elongated shape of the nanoparticles	$\chi_2 = A(625)/A(525)$	class 0: $\chi_1 < 1$
		class 1: $\chi_2 < 0.7$ (spherical)
		class 2: $\chi 2 > 0.7$ (elongated)
3. time of the nanoparticle formation	time τ when χ_1 becomes larger than 1	class 0: $\tau > 4000$ s
		class 1: 1500 s $< \tau <$ 4000 s
		class 2: $\tau < 1500$ s

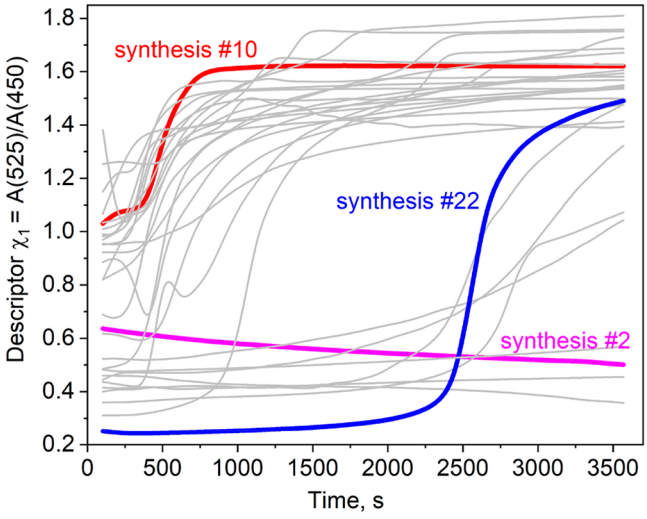

Figure 7. Time dependence of the χ_1 descriptor for different reactions specified in Table 1. Colors indicate three classes reported in Table 3 for τ.

synthesis with long induction period and incomplete growth even at the last measurement. Finally, the magenta curve (synthesis #2) indicates the reaction when the particles were not formed or the induction period was much longer than the observation time.

3.3. Results of the Classification. The quality of the ML approximation was evaluated in the Leave-One-Out cross-validation applied for the trained Extra Trees model. Good quality of classification can be intuitively understood when

https://doi.org/10.1021/acs.jpcc.2c06625
J. Phys. Chem. C XXXX, XXX, XXX−XXX

different classes are well separated from each other. We iterated over different combinations of two and three descriptors of synthesis to find those providing the best quality. Such combinations can be then interpreted as chemically more relevant. They highlight parameters of synthesis that affect the resulting spectra more. The best combinations of three descriptors are reported in Table 4.

Table 4. Selected Triples of the Descriptors of Synthesis Providing High Quality of the Classification for the Studied Descriptors of the Spectra: χ_1, χ_2, and τ (See Table 3 for Details)

combination of the descriptors of synthesis	accuracy
target: χ_1	
CTAB, Au, acid	0.60
CTAB, AA − CTAB,Au − AA	0.69
AA − CTAB, Au·AAAu − AA − CTAB	0.79
target: χ_2	
CTAB, Au, Acid	0.57
AA + CTAB, Au, Au·AA	0.75
Au + AA + CTAB, Au − AA ,Au − AA − CTAB	0.79
target: τ	
CTAB, Au, acid	0.70
CTAB,Au − AA + CTAB, Au − AA	0.82
Au·AA, Au − AA + CTAB ,Au − AA − CTAB	0.83

For all tasks, the combination of initial descriptors, [Au, AA, CTAB] provided a lower quality than other optimal combinations. The most frequent expression for the descriptors of synthesis with the good prediction quality contained the difference between Au and AA, product Au·AA, and the difference between Au and the sum of AA + CTAB. The addition of a nonlinear descriptor with multiplication of Au·AA increased the accuracy by up to 80% for χ_1. On the contrary, only linear combinations of Au, AA, and CTAB were sufficient to achieve highest accuracy for χ_2 and τ.

To achieve a lower bias of the ML model and thus its higher predictive capabilities, we have reduced the space of the descriptors of synthesis. Using 2 instead of 3 descriptors did not reduce the quality of the classification for χ_1 and τ. Figure 8 shows selected combinations of a couple of descriptors providing high LOOCV quality. The values of the descriptors along each axis in these figures were normalized prior to classification by subtracting the mean and dividing by standard deviation across the sample. Within linear combinations of the descriptors, the difference Au − AA and CTAB provided the best quality of classification. Addition of quadratic product Au·AA improved the quality up to 80% similar to the case of three descriptors in Table 4.

The areas of different classes for χ_2 are more difficult to separate in the 2d plane. This is explained by the fact that many different shapes of particles can be formed while we try to differentiate only the spherical and elongated ones with such descriptor. Another complication is the coexistence of several shapes in certain syntheses. Therefore, one descriptor of the spectrum may result in a crude classification. However, we achieved accuracy close to 70% as shown in Figure 8c, which is only 10% less compared to the classification with three descriptors. The syntheses with the longest induction period and mixtures without nanoparticles are grouped in the bottom right corner of the 2d map in Figure 8d. This corner is characterized by a lower amount of ascorbic acid as compared to Au and also lower amount of CTAB in the reaction mixture.

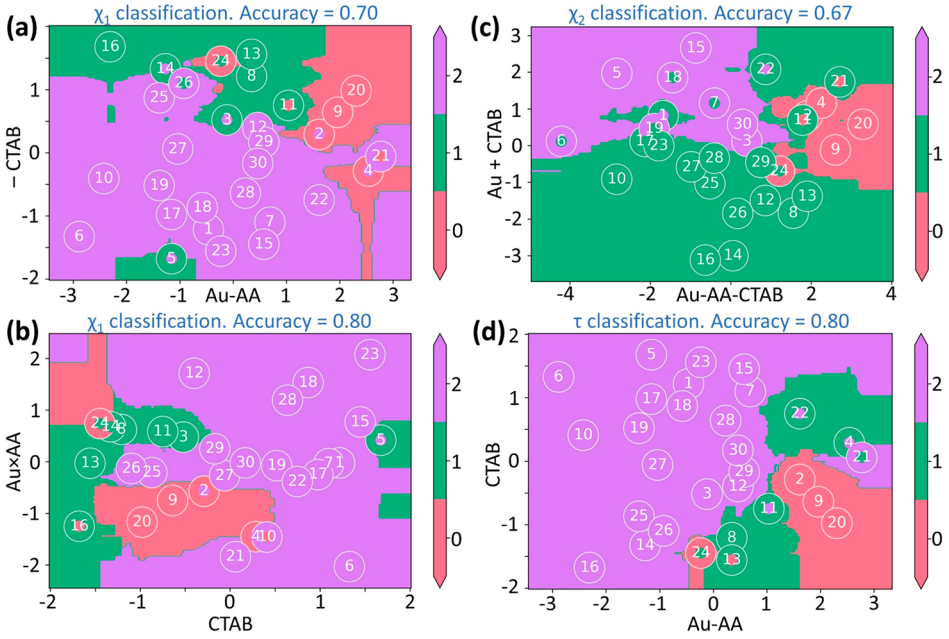

Figure 8. (a, b) Selected pairs of the descriptors of synthesis providing good accuracy for χ_1 classification. The values of the descriptors were normalized (subtracted mean and dividing by standard deviation) before the model training. (c) Pair of synthesis descriptors that provides good accuracy for χ_2 classification. (d) Selected pair of the descriptors of synthesis providing good accuracy for the τ classification (see Table 3 for the definition). Background colors visualize classes from Table 3. In panels a and b class 0 combines spectra with $\chi_1 < 1$, class 1—$1 < \chi_1 < 1.5$, class 2—$\chi_1 > 1.5$; in panel c, class 0 corresponds to $\chi_1 < 1$, i.e. no particles formed, class 1—($\chi_2 < 0.7$, spherical particles class 2—$\chi_2 > 0.7$, elongated particles; in panel d, class 0 combines slow reactions with $\tau > 4000$ s, class 1—reactions with period 1500 s $< \tau <$ 4000 s, class 2—fast reactions with $\tau < 1500$ s.

https://doi.org/10.1021/acs.jpcc.2c06625
J. Phys. Chem. C XXXX, XXX, XXX−XXX

The interpretation of the classification results in Figure 8 is related to the Au nanoparticle growth mechanism. In our protocol, we varied the amounts of the three reagents while keeping the concentrations of the acetone, Ag precursor, and cyclohexane fixed throughout the syntheses. Figure 8a indicates that a higher amount of CTAB along with a smaller amount of Au compared to AA favors the pronounced SPR maximum with large $\chi_1 = A(525)/A(450)$ (magenta region in the scatter plot). Ascorbic acid in the mixture of $HAuCl_4$ and CTAB mildly reduces Au(III) to Au(I), turning the solution colorless. The Au(I) complexes are trapped within CTAB micelles and further reduced by the electrons and radicals produced by radiolysis from acetone under UV irradiation.[59,60] When Au is in large excess compared to AA, the particles are not formed (red region in Figure 8a) with an exception for synthesis #21 where the amount of AA was less than Au but much higher than in the neighbor unsuccessful synthesis #4. This indicates that an excess of AA is not a necessary condition for the nanoparticle formation and the initial stage of Au^{III} reduction may be completed if some amount of seeds were formed in the solution and Au ions further reduce autocatalytically on the surface of the formed seeds. This is experimentally confirmed by observation of a disproportionation reaction between Au(0) and Au(III) catalyzed by seeds and catalytic reduction of Au(I) on the surface of seeds.[53] Parts a and b of Figures 8 also indicate the important role of CTAB concentration in the formation of NPs. Zhu et al.[61] note the large role of CTAB in the formation of gold nanoparticles. They suggest that the active species of $HAuCl_4$ interact with the positive headgroup of CTAB aggregates, and submicellar aggregates may be formed, which brings the reactants together through electrostatic interactions. In this way, the reaction takes place between ascorbic acid and solubilized CTA−$AuCl_4$ complex into the Stern layer of CTAB micelles (Scheme 1).[61]

Scheme 1. Steps of Gold Ions Reduction and the Reagents Affecting This Process

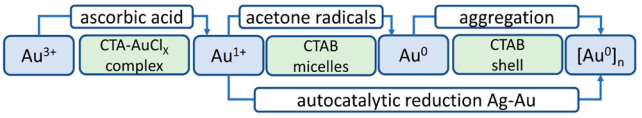

The availability of AA to reduce Au and the amount of CTAB, AA, and Au are important for the result of synthesis. As follows from Figure 8c the spherical shape (green color) is favorable for small amounts of Au + CTAB. For larger amounts of Au + CTAB, the result depends on the amount of Au with respect to AA + CTAB. In the excess of AA + CTAB, the elongated shape was preferable. In excess Au, the particles did not form (red region) or a spherical shape was preferable (syntheses #21, #22). These results can be understood in terms of interplay between available Ag ions, CTAB, and radicals in the reaction mixture. For a smaller amount of Au in the reaction mixture, the available Ag ions and CTA−Br−Ag^+ complexes preferentially reduce onto higher energy surface facets early in the reaction, leading to anisotropic growth.[31,62,63]

Finally, in Figure 8d, the reactions with excess AA compared to Au were faster. In the region of Au > AA, the result depends on the amount of CTAB. At low amount of CTAB (bottom red right corner), the particles do not form, while at larger amount of CTAB the formation was slowly completed even with a small amount of AA that may be attributed to the reduction capability of radicals formed under UV irradiation.[64] We have performed series of syntheses increasing only AA while keeping the Au and CTAB amounts constant (Table S2 and Figure S1 in Supporting Information). A smaller amount of AA results in a systematically longer induction period needed for the SPR peak formation. At too high AA concentrations (AA/Au > 3), the fast growth of the nanoparticles resulted in their larger dimensions. The obtained colloidal solution at these ratios was not stable forming a black precipitate.

One may argue the quality of classification in Figure 8 is not ideal. Despite these figures showing the optimal combinations of descriptors for the separation between classes, some controversial points still exist. This holds for the area with points #4 + #10 in Figure 8b, #4 + #21 in Figure 8a and #8, #29 + #24, and #2 + #11 in Figure 8c. This ambiguous classification may be attributed to the complexity of the reaction. The latter is described by a set of (nonlinear) differential equations that may exhibit unstable solutions. The small variations of initial conditions may significantly affect the outcome by varying the pathway of the reaction. Such problem may be understood with the mechanical analogy of the 3-body problem. If we try to predict positions and velocities of three bodies in the space knowing their initial positions and velocities, we would encounter a problem that for certain starting combinations and intervals of time the movement would be so complex that mapping a space would require too dense sampling of points. The same holds for complex chemical reactions. Therefore, we consider our results as a useful guide to the areas of reaction space where a detailed search could be performed. Increasing the size of the training set (e.g., by using automatized synthesis systems), the search of new descriptors may be extended to a more complex analytical expression. Resulting descriptors with a good classification accuracy would provide insights into general dependencies between the parameters of the reaction.

4. PROSPECT FOR DATA-HUNGRY APPROACHES

The discussion above deals with the limited size of data sets for ML algorithm training. The combination of the Extra Trees approach and Leave-One-Out cross-validation is already applicable for training sets containing several tens of entries.[57] However, in this study, we did not consider the effect of silver ions concentration and amount of acetone added, which increases the dimensionality of the parameter space to 5. Moreover, the region of interest for a certain reaction may be narrow and thus requires more points for sampling. While accurate sampling of the whole reaction space is beyond the scope of the present manuscript, we discuss a practical methodology applicable for fine sampling.

Microfluidic systems offer a unique possibility to carry out the reaction in a small volume. We have designed a setup to reproduce reaction conditions for the UV-mediated synthesis of gold nanoparticles in a flow regime. Figure 9a shows the main components of the setup, including syringe pumps (1), 3d printed chip (2) applied for mixing and slug generation, quartz capillary installed in front of UV lamp (3) for irradiation and in situ UV−vis cell (5). Further details of the experimental scheme are provided in the Supporting Information.

Each experiment in Table 1 required more than1 h to complete. The microfluidic setup can generate independent reaction conditions almost for each slug (see Figure 9a,

https://doi.org/10.1021/acs.jpcc.2c06625
J. Phys. Chem. C XXXX, XXX, XXX−XXX

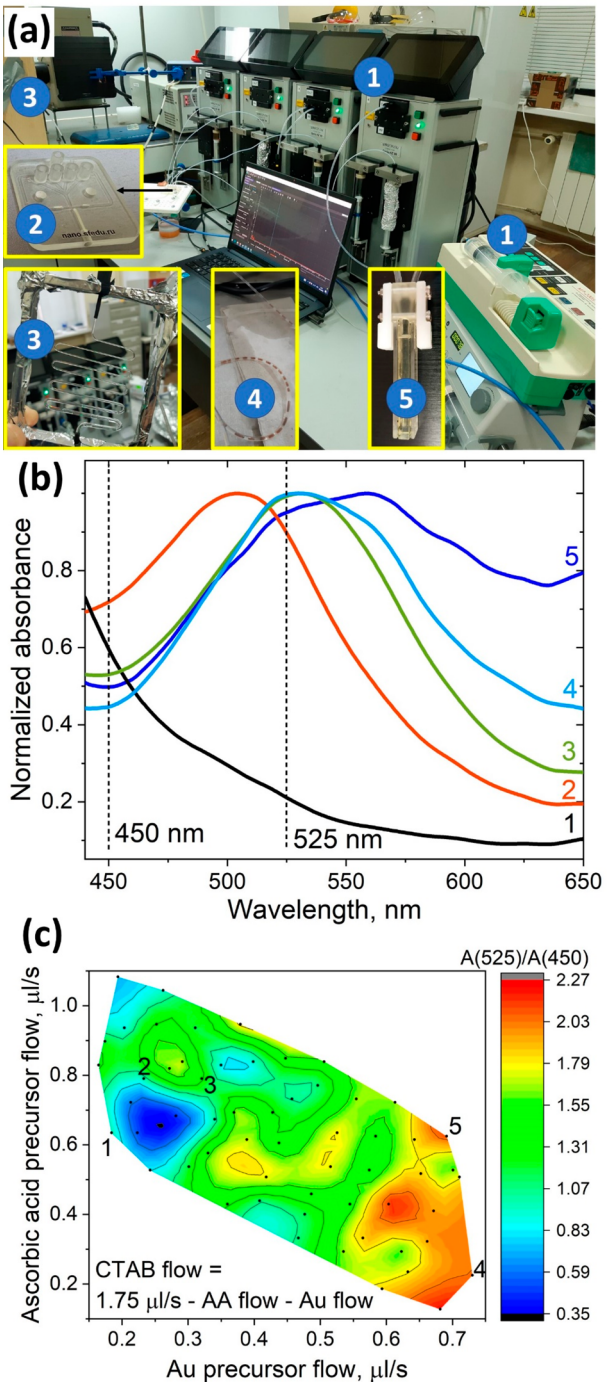

Figure 9. (a) Microfluidic setup for high-throughput screening of the reaction parameters: 1, syringe pumps; 2, mixer containing four inlets for reagents and one for oil carrier; 3, UV lamp and quartz capillary for irradiation; 4, the slugs of reaction mixture inside the tube; 5, couvette for UV−vis measurements of single slugs. (b) Selected UV−vis spectra from the slugs after UV irradiation. (c) Values of the absorbance ratio $A(525\ \text{nm})/A(450)$ for the 60 reaction points generated in a flow regime.

element 4). Thus, within 2 h, one can perform multiple experiments sending delayed slugs with different reaction mixtures to the capillary (element 3) for UV-irradiation. In the experiment, the oil carrier flow was set to 8.5 mL/h and the total flow of four reagents was 6.3 mL/h. The time between mixing and spectrum characterization could range from 15 to 60 min. Syringe 1 contained an aqueous solution of $NaAuCl_4 \cdot 4H_2O$ (2 mM in 25 mL); syringe 2, CTAB aqueous solution (50 mM in 25 mL, kept at 60 °C); syringe 3, L-ascorbic acid aqueous solution (2 mM in 25 mL); and syringe 4 contained an aqueous mixture of $AgNO_3$ and acetone (1.08 mM and 508 mM dissolved in 50 mL of water).

The system changed the parameters in an automated way. For a trial experiment, we have varied flows from syringes 1−3 in the range 0.15−0.735 μL/s, 0.15−0.735 μL/s, 0.03−1.2 μL/s. Flow 4 was fixed to 0.25 μL/s. Figure 9b shows typical spectra acquired during scanning of the relative flow speed of the reagents. For some combinations of flows, we have observed a plasmon peak shift toward lower wavelength, which was not observed in batch experiments. We attribute this shift to the formation of the AuAg alloy.[65] Figure 9c shows the scatterplot based on 60 UV−vis spectra from the slugs containing different ratios of metal salt and reducing and capping agents. The time required to perform 60 experiments for this map was less than 2 h compared to more than 60 h required for 30 batch experiments in the main text.

Though we encountered several technical difficulties upon transferring the reaction in flow (e.g., CTAB crystallization or acetone impact on the drop generation), we find such an approach useful for screening the experiments with long reaction time.

5. CONCLUSIONS

Time-consuming chemical reactions are difficult to repeat many times. Their transfer to high-throughtput microfluidic systems may also be not straightforward. Thus, the application of routine data-driven approaches for optimization is not straightforward. In this work, we demonstrate how useful insights may be obtained with machine learning already on a small data set. The effects of gold precursor, reducing agent, and surfactant were studied in a systematic way for UV-assisted formation of gold nanoparticles. The experimental points in the space of the reaction parameters were chosen via improved Latin hypercube sampling. By varying amounts of $HAuCl_4 \cdot 4H_2O$, ascorbic acid, and CTAB, we obtained spherical or elongated nanoparticles and monitored the reaction in situ with UV−vis spectroscopy. In total, 30 syntheses were performed in a wide range of relative amounts of the three reagents.

The series of resulting UV−vis spectra and their time evolution were a subject for ML analysis. Comparatively small amount of entries in the data set represents a challenge for conventional data-hungry approaches. Therefore, we performed dimensionality reduction and selected only informative features of spectra (normalized intensity of the surface plasmon resonance, asymmetry of the SPR maximum, and time for saturation of the SPR intensity) and informative features of synthesis. The latter were chosen iteratively from the manifold of algebraic expressions for amounts of Au, AA, and CTAB in the reaction using the cross-validation accuracy as a criterion. We addressed three questions about NPs formation and formulated them in terms of a classification problem with three classes: if the nanoparticles were formed during the synthesis, the spherical or elongated shape of the nanoparticles, and the time of the nanoparticle formation. The quality ~80% was achieved for each task using three descriptors and slightly reduced when reducing the number of descriptors to two. The most important descriptors of synthesis were as follows: the difference between the amounts

https://doi.org/10.1021/acs.jpcc.2c06625
J. Phys. Chem. C XXXX, XXX, XXX−XXX

of gold and ascorbic acid Au − AA, the amount of CTAB, the total amount of Au + CTAB, and the product Au·AA.

We believe that the descriptor-oriented approach would be useful for complex chemical tasks where a large data set of syntheses is difficult to obtain. For such cases, the use of simple ML models based on Extremely Randomized Trees avoids overfitting while preserving high approximation quality. The smallest combination of descriptors reduces the bias of the model and permits human-friendly visualization of the results on the 2d and 3d scatter plots.

■ ASSOCIATED CONTENT

Supporting Information

The Supporting Information is available free of charge at https://pubs.acs.org/doi/10.1021/acs.jpcc.2c06625.

UV−vis spectra measured in situ for all reported syntheses, TEM images for the synthesized particles, and details about manufacturing microfluidic setup for UV-assisted synthesis (PDF)

■ AUTHOR INFORMATION

Corresponding Author

Alexander A. Guda − *The Smart Materials Research Institute, Southern Federal University, 344090 Rostov-on-Don, Russia;* orcid.org/0000-0002-6941-4987; Email: guda@sfedu.ru

Authors

Mikhail V. Kirichkov − *The Smart Materials Research Institute, Southern Federal University, 344090 Rostov-on-Don, Russia*

Viktor V. Shapovalov − *The Smart Materials Research Institute, Southern Federal University, 344090 Rostov-on-Don, Russia*

Alexey I. Muravlev − *The Smart Materials Research Institute, Southern Federal University, 344090 Rostov-on-Don, Russia*

Danil M. Pashkov − *The Smart Materials Research Institute, Southern Federal University, 344090 Rostov-on-Don, Russia*

Sergey A. Guda − *The Smart Materials Research Institute, Southern Federal University, 344090 Rostov-on-Don, Russia; Institute of mathematics, mechanics and computer science, Southern Federal University, 344090 Rostov-on-Don, Russia;* orcid.org/0000-0002-2398-1847

Anton P. Bagliy − *The Smart Materials Research Institute, Southern Federal University, 344090 Rostov-on-Don, Russia; Institute of mathematics, mechanics and computer science, Southern Federal University, 344090 Rostov-on-Don, Russia*

Sergey A. Soldatov − *The Smart Materials Research Institute, Southern Federal University, 344090 Rostov-on-Don, Russia*

Sergey V. Chapek − *The Smart Materials Research Institute, Southern Federal University, 344090 Rostov-on-Don, Russia*

Alexander V. Soldatov − *The Smart Materials Research Institute, Southern Federal University, 344090 Rostov-on-Don, Russia*

Complete contact information is available at: https://pubs.acs.org/10.1021/acs.jpcc.2c06625

Notes

The authors declare no competing financial interest.

■ ACKNOWLEDGMENTS

The synthesis part of the research was supported by the Strategic Academic Leadership Program of the Southern Federal University ("Priority 2030"). A.A.G. and A.V.S. acknowledge the Ministry of Science and Higher Education of the Russian Federation for financial support (Agreement 075-15-2021-1363).

■ REFERENCES

(1) Chai, Y.; et al. Noble Metal Particles Confined in Zeolites: Synthesis, Characterization, and Applications. *Advanced Science* **2019**, *6* (16), 1900299.

(2) Otsuki, J.; Sugawa, K.; Jin, S. Plasmonic triangular nanoprism sensors. *Materials Advances* **2021**, *2* (1), 32−46.

(3) Ahmed, H. M.; et al. Applications of Nanomaterials in Agrifood and Pharmaceutical Industry. *J. Nanomater.* **2021**, *2021*, 1.

(4) Mo, Y.; et al. Gold nano-particles (AuNPs) carrying miR-326 targets PDK1/AKT/c-myc axis in hepatocellular carcinoma. *Artificial Cells, Nanomedicine and Biotechnology* **2019**, *47* (1), 2830−2837.

(5) Zheng, G.; et al. Discrete metal nanoparticles with plasmonic chirality. *Chem. Soc. Rev.* **2021**, *50* (6), 3738−3754.

(6) Wang, Y.; et al. Zeolite Fixed Metal Nanoparticles: New Perspective in Catalysis. *Acc. Chem. Res.* **2021**, *54* (11), 2579−2590.

(7) Yang, J.; et al. Enhanced Catalytic Performance through In Situ Encapsulation of Ultrafine Ru Clusters within a High-Aluminum Zeolite. *ACS Catal.* **2022**, *12* (3), 1847−1856.

(8) Adamcsik, B.; et al. Palladium nanoparticles on a pyridinium supported ionic liquid phase: a recyclable and low-leaching palladium catalyst for aminocarbonylation reactions. *RSC Adv.* **2020**, *10*, 23988−23998.

(9) Matátková, O.; et al. Antimicrobial properties and applications of metal nanoparticles biosynthesized by green methods. *Biotechnology Advances* **2022**, *58*, 107905.

(10) Ullah, S.; et al. Palladium nanoparticles synthesis, characterization using glucosamine as the reductant and stabilizing agent to explore their antibacterial & catalytic applications. *Microbial pathogenesis* **2018**, *125*, 150−157.

(11) Umar, A.; Kim, J.; Choi, S.-M. One-Pot Synthesis of Monodisperse Single-Crystalline Spherical Gold Nanoparticles for Universal Seeds. *Cryst. Growth Des.* **2021**, *21* (7), 4133−4140.

(12) Zheng, Y.; et al. Synthesis of Branched Au-PdAg Hybrid Nanosheets by Controlled Reduction in a Galvanic Replacement Reaction. *ChemNanoMat* **2021**, *7* (11), 1205−1212.

(13) Xu, H.; et al. Alcohol Sensor Based on Surface Plasmon Resonance of ZnO Nanoflowers/Au Structure. *Materials* **2022**, *15* (1), 189.

(14) Pakravan, A.; Salehi, R.; Mahkam, M. Comparison study on the effect of gold nanoparticles shape in the forms of star, hallow, cage, rods, and Si-Au and Fe-Au core-shell on photothermal cancer treatment. *Photodiagnosis and Photodynamic Therapy* **2021**, *33*, 102144.

(15) Dejpasand, M. T.; et al. Surface plasmon-induced photodegradation of methylene blue with single layer graphene quantum dots/Au nanospheres under visible-light irradiation. *J. Alloys Compd.* **2021**, *885*, 160904.

(16) Guo, Y.; et al. Ag-Au Core-Shell Triangular Nanoprisms for Improving p-g-C3N4 Photocatalytic Hydrogen Production. *Nanomaterials* **2021**, *11* (12), 3347.

(17) Zhang, D.; et al. Room-Temperature Benzene Sensing with Au-Doped ZnO Nanorods/Exfoliated WSe2 Nanosheets and Density Functional Theory Simulations. *ACS Appl. Mater. Interfaces* **2021**, *13* (28), 33392−33403.

(18) Turkevich, J.; Stevenson, P. C.; Hillier, J. A study of the nucleation and growth processes in the synthesis of colloidal gold. *Discuss. Faraday Soc.* **1951**, *11* (0), 55−75.

(19) Gao, Y.; Torrente-Murciano, L. Mechanistic insights of the reduction of gold salts in the Turkevich protocol. *Nanoscale* **2020**, *12* (4), 2740−2751.

(20) Matamoros-Ambrocio, M.; et al. A Comparative Study of Gold Impregnation Methods for Obtaining Metal/Semiconductor Nano-

photocatalysts: Direct Turkevich, Inverse Turkevich, and Progressive Heating Methods. *Catalysts* **2018**, *8* (4), 161.
(21) Akbarzadeh Khiavi, M.; Safary, A.; et al. PEGylated gold nanoparticles-ribonuclease induced oxidative stress and apoptosis in colorectal cancer cells. *Bioimpacts* **2020**, *10* (1), 27−36.
(22) Damilos, S.; et al. Continuous citrate-capped gold nanoparticle synthesis in a two-phase flow reactor. *Journal of Flow Chemistry* **2021**, *11*, 553−567.
(23) Sen, N.; et al. Flow synthesis of PVP capped gold nanoparticles in capillary microreactor. *Chemical Engineering and Processing - Process Intensification* **2022**, *179*, 109036.
(24) Lang, E. N.; et al. Oleylamine Impurities Regulate Temperature-Dependent Hierarchical Assembly of Ultranarrow Gold Nanowires on Biotemplated Interfaces. *ACS Nano* **2021**, *15* (6), 10275−10285.
(25) Nguyen, T. H. A.; et al. Novel biogenic silver and gold nanoparticles for multifunctional applications: Green synthesis, catalytic and antibacterial activity, and colorimetric detection of Fe(III) ions. *Chemosphere* **2022**, *287*, 132271.
(26) Vinay, S. P.; et al. In-vitro antibacterial, antioxidant and cytotoxic potential of gold nanoparticles synthesized using novel Elaeocarpus ganitrus seeds extract. *Journal of Science: Advanced Materials and Devices* **2021**, *6* (1), 127−133.
(27) Do Thi, H.; Nghien Thi Ha, L.; Chu Viet, H. Seeded Growth Synthesis of Uniform Gold Nanoparticles with Controlled Diameters up to 220 nm. *J. Electron. Mater.* **2021**, *50* (10), 5514−5521.
(28) Rashid, T. M.; et al. Synthesis and characterization of Au:ZnO (core:shell) nanoparticles via laser ablation. *Optik* **2021**, *244*, 167569.
(29) Ohara, Y.; et al. Seed-mediated gold nanoparticle synthesis via photochemical reaction of benzoquinone. *Colloids Surf., A* **2020**, *586*, 124209.
(30) Rodríguez, G. R. C.; et al. Effect of pH and chloroauric acid concentration on the geometry of gold nanoparticles obtained by photochemical synthesis. *Journal of Physics: Conference Series* **2017**, *935*, 012027.
(31) Kim, F.; Song, J. H.; Yang, P. Photochemical Synthesis of Gold Nanorods. *J. Am. Chem. Soc.* **2002**, *124* (48), 14316−14317.
(32) Kim, F.; Song, J.; Yang, P. Photochemical Synthesis of Gold Nanorods. *J. Am. Chem. Soc.* **2002**, *124*, 14316−7.
(33) Perez-Lloret, M.; et al. One-Step Photochemical Green Synthesis of Water-Soluble Ag, Au and Au@Ag Core-Shell Nanoparticles. *Chem. Eur. J.* **2019**, *25*, 14638.
(34) Habibullah, G.; Viktorova, J.; Ruml, T. Current Strategies for Noble Metal Nanoparticle Synthesis. *Nanoscale Res. Lett.* **2021**, *16* (1), 47.
(35) Lei, M.; et al. Size-Controlled Au Nanoparticles Incorporating Mesoporous ZnO for Sensitive Ethanol Sensing. *ACS Appl. Mater. Interfaces* **2021**, *13* (44), 51933−51944.
(36) Awwad, N. S.; et al. Green synthesis of different ratios from bimetallic gold: Silver nanoparticles core@shell via laser ablation scattered in Chitosan-PVA matrix and its electrical conductivity behavior. *Compos. Commun.* **2021**, *24*, 100678.
(37) Burrows, N. D.; et al. Understanding the Seed-Mediated Growth of Gold Nanorods through a Fractional Factorial Design of Experiments. *Langmuir: the ACS journal of surfaces and colloids* **2017**, *33* (8), 1891−1907.
(38) Tao, H.; et al. Nanoparticle synthesis assisted by machine learning. *Nat. Rev. Mater.* **2021**, *6* (8), 701−716.
(39) Mekki-Berrada, F.; et al. Two-step machine learning enables optimized nanoparticle synthesis. *npj Computational Materials* **2021**, *7* (1), 55.
(40) Pellegrino, F.; et al. Machine learning approach for elucidating and predicting the role of synthesis parameters on the shape and size of TiO2 nanoparticles. *Sci. Rep.* **2020**, *10* (1), 18910.
(41) Wahl, C. B. Machine learning-accelerated design and synthesis of polyelemental heterostructures. *Science Advances* **2021**, *7* (52), No. eabj5505.
(42) Gherman, A. M. R.; et al. Artificial neural networks modeling of the parameterized gold nanoparticles generation through photo-induced process. *Materials Research Express* **2018**, *5*, 085011.
(43) Li, J.; et al. Deep Learning Accelerated Gold Nanocluster Synthesis. *Advanced Intelligent Systems* **2019**, *1* (3), 1900029.
(44) Haiss, W.; et al. Determination of Size and Concentration of Gold Nanoparticles from UV−Vis Spectra. *Anal. Chem.* **2007**, *79* (11), 4215−4221.
(45) Kirichkov, M. X-ray and optical characterization of the intermediate products in the Au3+ reduction process by oleylamine. *Radiat. Phys. Chem.* **2020**, *175*, 108067.
(46) Chen, X.; et al. Insights into Growth Kinetics of Colloidal Gold Nanoparticles: In Situ SAXS and UV−Vis Evaluation. *J. Phys. Chem. C* **2021**, *125* (1), 1087−1095.
(47) Polte, J.; et al. Mechanism of Gold Nanoparticle Formation in the Classical Citrate Synthesis Method Derived from Coupled In Situ XANES and SAXS Evaluation. *J. Am. Chem. Soc.* **2010**, *132* (4), 1296−1301.
(48) Pashkov, D. M.; et al. Quantitative Analysis of the UV−Vis Spectra for Gold Nanoparticles Powered by Supervised Machine Learning. *J. Phys. Chem. C* **2021**, *125* (16), 8656−8666.
(49) Sanabria-Cala, J. A.; et al. Gold Nanoparticles Formation Mechanism by Photochemical Synthesis. *Chemical Engineering Transactions* **2018**, *64*, 402.
(50) Geurts, P.; Ernst, D.; Wehenkel, L. Extremely randomized trees. *Machine Learning* **2006**, *63* (1), 3−42.
(51) King, S. R.; Massicot, J.; McDonagh, A. M. A Straightforward Route to Tetrachloroauric Acid from Gold Metal and Molecular Chlorine for Nanoparticle Synthesis. *Metals* **2015**, *5* (3), 1454−1461.
(52) Elding, L.; et al. Kinetics, Mechanism and Equilibria for Halide Substitution Processes of Chloro Bromo Complexes of Gold(III). *Acta Chemica Scandinavica. Series B: Organic chemistry and biochemistry* **1978**, *32a*, 867−877.
(53) Scarabelli, L.; et al. A "Tips and Tricks" Practical Guide to the Synthesis of Gold Nanorods. *J. Phys. Chem. Lett.* **2015**, *6* (21), 4270−4279.
(54) Khan, Z.; et al. Au(III)−CTAB reduction by ascorbic acid: Preparation and characterization of gold nanoparticles. *Colloids Surf., B* **2013**, *104*, 11−17.
(55) Zhang, Q.; et al. Intertwining Roles of Silver Ions, Surfactants, and Reducing Agents in Gold Nanorod Overgrowth: Pathway Switch between Silver Underpotential Deposition and Gold−Silver Codeposition. *Chem. Mater.* **2016**, *28* (8), 2728−2741.
(56) Pong, B.-K.; et al. New Insights on the Nanoparticle Growth Mechanism in the Citrate Reduction of Gold(III) Salt: Formation of the Au Nanowire Intermediate and Its Nonlinear Optical Properties. *J. Phys. Chem. C* **2007**, *111* (17), 6281−6287.
(57) Trummer, D.; et al. Deciphering the Phillips Catalyst by Orbital Analysis and Supervised Machine Learning from Cr Pre-edge XANES of Molecular Libraries. *J. Am. Chem. Soc.* **2021**, *143* (19), 7326−7341.
(58) Chang, S.-S.; et al. The Shape Transition of Gold Nanorods. *Langmuir* **1999**, *15* (3), 701−709.
(59) Zech, T.; et al. Investigating Growth of Gold Nanorods by Simultaneous Small-Angle X-Ray and Neutron Scattering. *Particle & Particle Systems Characterization* **2022**, *39* (3), 2100172.
(60) Abidi, W.; et al. One-Pot Radiolytic Synthesis of Gold Nanorods and Their Optical Properties. *J. Phys. Chem. C* **2010**, *114* (35), 14794−14803.
(61) Zhu, H.; et al. Experimental and theoretical studies on the role of silver in gold nanorods growth. *J. Nanopart. Res.* **2017**, *19* (5), 183.
(62) Moreau, L. M.; et al. The role of trace Ag in the synthesis of Au nanorods. *Nanoscale* **2019**, *11* (24), 11744−11754.
(63) Xu, Y.; et al. Cooperative interactions among CTA+, Br− and Ag+ during seeded growth of gold nanorods. *Nano Research* **2017**, *10* (6), 2146−2155.
(64) Tang, J.; Huang, J.; Man, S.-Q. Preparation of gold nanoparticles by surfactant-promoted reductive reaction without extra reducing agent. *Spectrochimica Acta Part A: Molecular and Biomolecular Spectroscopy* **2013**, *103*, 349−355.

https://doi.org/10.1021/acs.jpcc.2c06625
J. Phys. Chem. C XXXX, XXX, XXX−XXX

(65) Malathi, S.; et al. One pot green synthesis of Ag, Au and Au−Ag alloy nanoparticles using isonicotinic acid hydrazide and starch. *Carbohydr. Polym.* **2014**, *111*, 734−743.

https://doi.org/10.1021/acs.jpcc.2c06625
J. Phys. Chem. C XXXX, XXX, XXX−XXX